PHYSICAL REVIEW B VOLUME 55, NUMBER 5 1 FEBRUARY 1997-I

Isotope effects on the optical phonons of $YBa_2Cu_3O_7$: Eigenvector and infrared charge determination

R. Henn, T. Strach, E. Schönherr, and M. Cardona
Max-Planck-Institut für Festkörperforschung, Heisenbergstrasse 1, 70569 Stuttgart, Germany

(Received 13 August 1996)

Using Raman spectroscopy and far-infrared ellipsometry we have investigated several $YBa_2Cu_3O_7$ ceramics which were made from different isotopically pure Cu or Ba precursors. The observed shifts of Raman- and infrared-active phonons reveal insight into their relative Ba and Cu normal mode content. This allows us to examine mode eigenvectors obtained from lattice dynamical calculations. Our Raman results demonstrate that the 121 cm^{-1} and 153 cm^{-1} A_g phonons are only very weakly mixed and represent almost pure Ba and Cu vibrations, respectively, whereas they suggest considerable Ba-Cu-O mixing in the case of the B_{2g} and B_{3g} phonons at 140 cm^{-1} and 142 cm^{-1}. The analysis of the infrared-active B_{1u} modes yields a substantial contribution of Cu to the 150 cm^{-1} and the 280 cm^{-1} phonons and of Ba to the 150 cm^{-1} mode. Making use of proposed eigenvectors, which are shown to be compatible with the observed isotope shifts, we determine effective charges for all ions from measured infrared oscillator strengths on a $YBa_2Cu_3O_7$ crystal. We find that the proposed eigenvectors are compatible with earlier experiments of the oxygen isotope effect as well as the replacement of Y by rare earth elements. [S0163-1829(97)02205-4]

I. INTRODUCTION

The chemical complexity of the high-temperature superconductors makes the determination and assignment of phononic features in these materials a difficult task. As an example $YBa_2Cu_3O_7$, with 13 atoms in its unit cell, has 39 phonon branches. Group theory predicts that the 36 optical phonons at the center of the Brillouin zone fall into six symmetry classes ($5\times A_g$, $5\times B_{2g}$, $5\times B_{3g}$, $7\times B_{1u}$, $7\times B_{2u}$, and $7\times B_{3u}$ in D_{2h} symmetry), with all phonons being either Raman (the 15 ''*g*'' modes) or infrared (the 21 ''*u*'' modes) allowed.[1] The symmetry class of a phonon can be determined experimentally by its dependence on light polarization in infrared or Raman spectra. If several phonons with the same symmetry exist any of these phonons may be a linear combination of all atomic vibrations of its symmetry class. It is thus not clear *a priori*, whether these phonons correspond to the motion of atoms of a single type or of several types of atoms in the unit cell. In fact, infrared-active modes must always be mixed modes to fulfill the requirement of zero motion of the center of mass of the unit cell. As a consequence, experimental information beyond the polarization dependence of each mode is required for a proper eigenvector assignment. However, experiments addressing the determination of phonon eigenvectors are rare. For the relatively simple situation (compared to high-T_c compounds) in the diatomic compound GaAs, neutron scattering has been demonstrated to be useful for the eigenvector determination of the modes at the X point.[2] Concerning eigenvectors of optical modes in high-T_c compounds, most experimental information is obtained by replacing certain elements in the unit cell by other chemically equivalent elements and analyzing the effect of this on the optical modes.[3,4] Easiest to interpret is the special case of isotopic substitution, since one can study the influence of the mass of a certain element in the unit cell on the vibrational spectrum without any change of the electronic properties of the solid.

In the simplest scenario only ions of one sublattice participate in a harmonic lattice vibration; the mass dependence of the mode frequency is then given by $1/\sqrt{m}$. In the case of mixed vibrations, where ions of several sublattices participate in the phonon motion, one expects only a partial isotope shift when ions of one sublattice are replaced by another isotope. In addition to this ''harmonic'' shift there may be smaller contributions due to anharmonicity and isotopic disorder.[5] These effects, which might also influence the phonon linewidth, can be observed in single crystals of very high quality. However, they are usually quite small and likely to be too weak to be observed in the high-T_c materials.

There have already been several reports about isotopic phonon shifts in high-T_c superconductors. The majority of these reports deals with the replacement of ^{16}O by ^{18}O which can even be substituted in a site-selective way.[4,6–9] For the heavier elements Y, Ba, and Cu the number of reports is scarce. Mascarenhas *et al.*[10] and Irwin *et al.*[11] have compared Raman spectra of $YBa_2{}^{nat}Cu_3O_7$ and $YBa_2{}^{65}Cu_3O_7$ ceramics. They found that only the 151 cm^{-1} A_g mode shifts in frequency and that it therefore involves mostly Cu displacements. In a previous study we quantitatively investigated the coupling of Ba ($\approx$121 cm^{-1}) and Cu vibrations for two A_g modes and found that the mixing does not exceed 20%, both at 300 K and at 10 K.[12] To our knowledge no infrared measurements on Ba or Cu isotopically substituted $YBa_2Cu_3O_7$ have yet been reported.

In this paper we present Raman measurements on ceramics with different Ba isotopes and results obtained by far-infrared ellipsometry on ceramics with different Ba and Cu isotopes. We confirm our earlier Raman results for the effect of Cu substitution. The experimental results compare well with eigenvectors obtained from semiempirical lattice dynamical calculations.[13,14] Making use of these eigenvectors we determine effective charges for all atoms in the unit cell

0163-1829/97/55(5)/3285(12)/$10.00

TABLE I. Isotopic composition and average mass of Ba and Cu in the $YBa_2Cu_3O_7$ ceramics used in this study.

Sample	Cu Isotopic composition	Av. mass	Ba Isotopic composition	Av. mass
Cu63	99.9% ^{63}Cu, 0.1% ^{65}Cu	62.93	nat.[a]	137.33
Cu65	0.3% ^{63}Cu, 99.7% ^{65}Cu	64.92	nat.[a]	137.33
Ba134	nat.[b]	63.55	83.1% ^{134}Ba, 7.62% ^{135}Ba, 1.64% ^{136}Ba, 1.35% ^{137}Ba, 6.29% ^{138}Ba	134.30
Ba138	nat.[b]	63.55	0.04 % ^{135}Ba, 0.07 % ^{136}Ba, 0.19 % ^{137}Ba, 99.7 % ^{138}Ba	137.91

[a] nat. Cu consists of 69.1% ^{63}Cu and 30.9% ^{65}Cu.

[b] nat. Ba consists of 0.1% ^{130}Ba, 0.1% ^{132}Ba, 2.4% ^{134}Ba, 6.6% ^{135}Ba, 7.8% ^{136}Ba, 11.3% ^{137}Ba, and 71.7% ^{138}Ba.

from measured oscillator strengths of the infrared-active B_{1u} modes of a $YBa_2Cu_3O_7$ crystal.

II. EXPERIMENT

A. Sample preparation

In contrast to oxygen, which diffuses easily in and out of $YBa_2Cu_3O_7$ ceramics at temperatures far below the melting point, the incorporation of Y, Ba, or Cu is only possible during the growth process. Thus for a comparative study several samples have to be synthesized from different isotopically pure starting materials. $YBa_2Cu_3O_{7-\delta}$ ceramics were produced from stoichiometric amounts of the appropriate oxides[15] using standard techniques.[16,17] We prepared four different samples. Two, which were also used in our previous investigation of the Cu-Ba A_g-mode coupling[12] contained either isotopically pure ^{63}Cu or ^{65}Cu, and natural Y, Ba, and O. The CuO source material was obtained by oxidizing sheets of Cu metal in flowing oxygen at 890 °C. For homogenization the procedure was stopped three times, the product ground, and annealed again. Two samples were produced from precursors containing isotopically pure ^{134}Ba and ^{138}Ba. Again, the remaining constituents were natural elements. Because of the small available amounts of isotopic source materials, the constituents (CuO, $BaCO_3$, Y_2O_3) were manually ground for 2 h. All samples were prepared under identical growth conditions, sintered, ground and pressed into cylindrical pellets of 8 mm diameter and 2 mm height. The average grain size of the microcrystals was around 2 μm. The isotopic characteristics of the four samples are summarized in Table I. In the following we shall label the samples as in Table I.

In order to exclude the possibility of phonon shifts due to different oxygen stoichiometry, an effect which could easily obscure the small shifts expected as a result of isotopic exchange, Raman spectra were taken for all four samples in the energy range from 400 cm^{-1} to 550 cm^{-1} (Fig. 1). In this region all four samples show two oxygen-related peaks with A_g symmetry at 440 cm^{-1} and 505 cm^{-1} which do not shift in energy to within ± 1 cm^{-1} for both pairs of samples. From their positions we conclude that all samples are fully oxygenized $YBa_2Cu_3O_{7-\delta}$, with δ close to zero (<0.05).[18]

B. Measurements

Raman measurements were performed with a multichannel spectrometer equipped with a charge-coupled device (CCD) detector. We used the 647.1 nm red laser line of a Kr/Ar-ion mixed-gas laser as excitation source. With this setup the spacing between adjacent pixels on the CCD corresponds to an energy difference of 0.5 cm^{-1}. This ensures that the observed phonons are dispersed over a large number of CCD channels and that their position and width can be determined accurately. The samples were mounted on the cold finger of a closed-cycle He cryostat allowing measurements in the temperature range from 10 to 300 K. The diameter of the laser spot on the sample was around 50 μm, much larger than the average grain size of the ceramics. Therefore the recorded spectra always represent an average over all

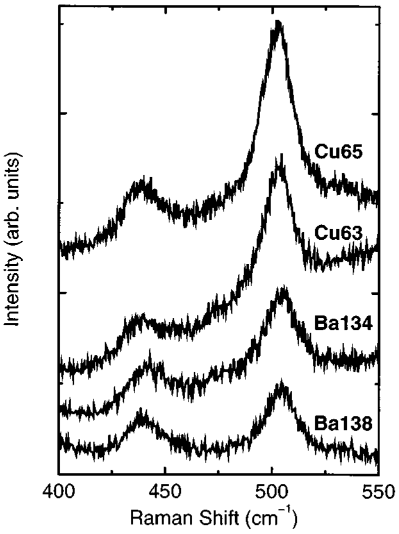

FIG. 1. Oxygen A_g phonons at 10 K of $YBa_2Cu_3O_7$ ceramics with different Cu and Ba isotopic compositions given in Table I.

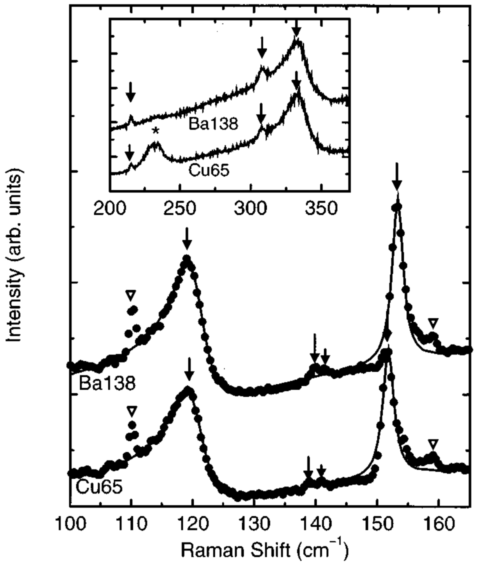

FIG. 2. Raman spectrum of samples Ba138 and Cu65 at 10 K excited with the 647.1 nm Kr^+ laser line. The triangles indicate plasma lines. The inset shows the same spectra at higher frequencies. The phonons investigated in this work are marked with arrows. The peak at about 230 cm^{-1} (marked with an asterisk) is most likely related to traces of the impurity phase $BaCuO_2$ (Ref. 23).

possible scattering configurations; spectra taken on different spots of the same sample are identical. For absolute wavelength calibration and to correct for small drifts of the spectrometer during the experiment, we used the very sharp and strong plasma lines of the Kr/Ar laser below 100 cm^{-1}. This method allowed us to limit deviations in Raman shifts between any two spectra to less than 0.1 cm^{-1}.

Far-infrared ellipsometric measurements were performed with a homebuilt ellipsometer attached to a Bruker 113v Fourier transform infrared spectrometer.[19] By applying this novel technique[20] we can overcome two main problems inherent to the competing reflectance technique: the reference problem and the related phase problem.[21] Ellipsometry is self-normalizing and reveals directly the complex dielectric function without requiring any Kramers-Kronig analysis. The samples were mounted on the cold finger of a continuous He flow cryostat and their temperature could be varied between 10 and 300 K. The quantity measured in ellipsometry is the complex reflectance ratio

$$\tilde{\rho}(\omega,\phi)=\frac{\tilde{r}_p(\omega,\phi)}{\tilde{r}_s(\omega,\phi)}, \tag{2.1}$$

where ϕ is the angle of incidence (in our experiment 80°, with a beam divergence of $\pm 2.0°$) and $\tilde{r}_p$ and $\tilde{r}_s$ are the Fresnel reflection coefficients for p- and s-polarized light, respectively.[22] The inversion of Eq. (2.1) yields directly the complex dielectric function:

$$\tilde{\epsilon}(\omega)=\left(\frac{1-\tilde{\rho}(\omega,\phi)}{1+\tilde{\rho}(\omega,\phi)}\right)^2\tan^2\phi\sin^2\phi+\sin^2\phi, \tag{2.2}$$

where an isotropic, clean, and homogeneous sample surface is assumed. This assumption is reasonable since for ceramic grains all possible orientations contribute to the measured signal. In order to cover the whole frequency range from 100 to 700 cm^{-1} we measured spectra with two different sets of beam splitters and filters (150–350, 300–700 cm^{-1}) at each temperature. All infrared spectra were taken with the resolution of 0.5 cm^{-1}.

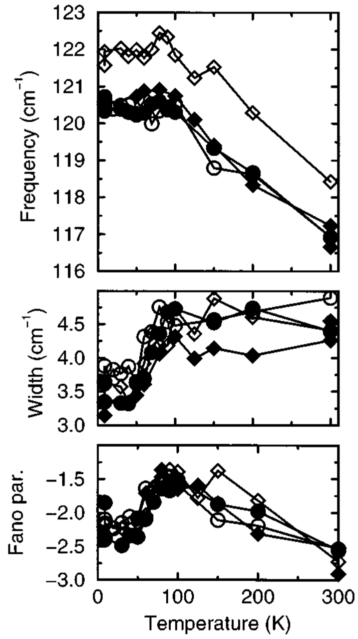

FIG. 3. Frequency, width and asymmetry parameter of the 121 cm^{-1} phonon as function of temperature for the four ceramic samples under study. The data correspond to Cu63 (open circles), Cu65 (filled circles), Ba134 (open diamonds), and Ba138 (filled diamonds), respectively. The lines joining the points are guides to the eye.

III. RESULTS

A. Raman spectroscopy

Figure 2 shows a typical Raman spectrum of an $YBa_2Cu_3O_{7-\delta}$ ceramic measured at 10 K in the energy range from 100 cm^{-1} to 400 cm^{-1}. The three strongest peaks with energies of 121 cm^{-1}, 153 cm^{-1}, and 337 cm^{-1}, correspond to three of the five expected A_g phonons of the $YBa_2Cu_3O_7$ structure, as observed in polarization-dependent Raman measurements on single crystals.[1] In addition to these peaks some smaller structures at 108, 140, 142, 158, 215, and 308 cm^{-1} can also be seen. The two sharp features at 108 and 158 cm^{-1} are laser plasma lines, the others correspond to $YBa_2Cu_3O_7$ phonons with B_{2g} and B_{3g} symmetry.[25]

For an exact determination of the positions and widths of the strong A_g phonons at 121 cm^{-1} and 153 cm^{-1} we fitted them with a Fano[24] and a Lorentzian line shape, respectively. Additionally a linear background was included. As seen in the figure, the fits describe the experimental spectra very well, except for the asymmetry of the 153 cm^{-1} peak which is not reproduced by the fit. The uncertainty in the values determined for the peak positions caused by signal noise and limitations in determining the drifts in the energy scale between spectra is around ± 0.15 cm^{-1} for the 10 K spectra (recording time 5 h). At higher temperatures we chose

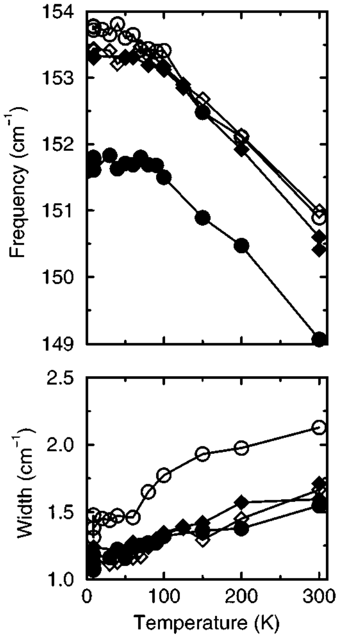

FIG. 4. Position and width of the 153 cm^{-1} phonon as function of temperature for the four studied ceramics. The data correspond to Cu63 (open circles), Cu65 (filled circles), Ba134 (open diamonds), and Ba138 (filled diamonds), respectively. The lines joining the experimental points are guides to the eye.

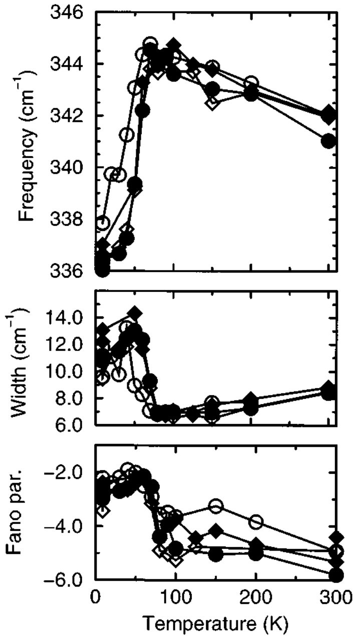

FIG. 5. Frequency, width and asymmetry parameter of the 337 cm^{-1} phonon as function of temperature for the four studied ceramics. The points correspond to Cu63 (open circles), Cu65 (filled circles), Ba134 (open diamonds), and Ba138 (filled diamonds), respectively. The lines joining the experimental points are guides to the eye.

shorter accumulation times (1 h), a fact which increased the uncertainty of the fitted values for the peak positions to ± 0.3 cm^{-1}.

Figures 3 and 4 summarize the results of least-squares fits to these phonons. In Fig. 3 the position, width, and Fano asymmetry parameter q of the 121 cm^{-1} phonon are plotted as a function of temperature for the four samples studied. This phonon shows a pronounced anomaly in width as well as asymmetry below the superconducting transition temperature T_c,[26] which is close to 90 K in these samples. This effect appears to be identical in all four samples. This is not the case for the frequency of the phonon: at all temperatures it is about 1.5 cm^{-1} higher in sample Ba134 than in the other three specimen which show identical values within the experimental accuracy. Position and width of the A_g phonon at 153 cm^{-1} are recorded as a function of temperature for all samples in Fig. 4. The position of the phonon is highest in the Cu63 sample and lowest in the Cu65 sample, with the positions in the other two samples being close to, but systematically below that in the Cu63 sample. The phonon is clearly broader in sample Cu63 than in the other three samples where it appears to be identical at all temperatures. The larger width probably corresponds to an increased lattice disorder in this ceramic caused by an additional preparation cycle of grinding, pressing and sintering which was applied only to this sample.

One should note that the results presented in our previous publication[12] were obtained on a different spectrometer using a different laser line as excitation source. This makes a detailed comparison of our new data with the previous spectra difficult. In particular, the high relative positional accuracy of 0.1 cm^{-1} between two spectra can only be achieved by calibrating to specific laser plasma lines. These lines are different for different laser wavelengths. Also, the observed phonons show strong changes in lineshape and intensity when the laser wavelength is changed.[27] Thus the *absolute* values of the phonon frequencies reported here differ slightly from our results in our previous report. The conclusions based on the observed *relative* shifts, however, remain unaffected.

In addition to the two A_g phonons at 121 cm^{-1} and 153 cm^{-1} we have also fitted the A_g phonon of the plane oxygen

TABLE II. Fitted positions of the Raman phonons observed at 10 K in the four samples studied. All phonons were fitted with Lorentzian profiles, except for the first one which was fitted with a Fano line shape.

	Frequency (cm^{-1})								
Sample	A_g	B_{3g}	B_{2g}	A_g	B_{2g}	B_{3g}	A_g	A_g	A_g
Cu63	120.6	140.2	141.6	153.8	215.1	307.6	338	437	503
Cu65	120.4	138.9	140.9	151.7	215.1	307.5	336	439	502
Ba134	121.9	139.7	141.9	153.4	215.3	308.0	337	442	504
Ba138	120.6	139.8	141.5	153.3	215.1	307.5	337	440	504

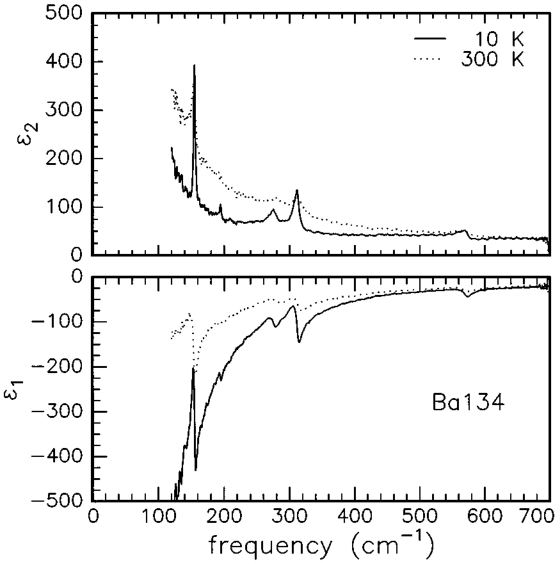

FIG. 6. Real [$\epsilon_1(\omega)$] and imaginary [$\epsilon_2(\omega)$] parts of the dielectric function obtained by ellipsometry for the Ba134 sample at 10 and 300 K.

(out of phase) at 337 cm^{-1} with a Fano line shape. Results are shown in Fig. 5. This phonon exhibits a strong anomaly in position, width, and asymmetry below the superconducting transition temperature T_c.[1,3] The anomaly is shifted downwards by roughly 15 K in sample Cu63 in comparison to the other three samples which appear again identical within experimental uncertainty.

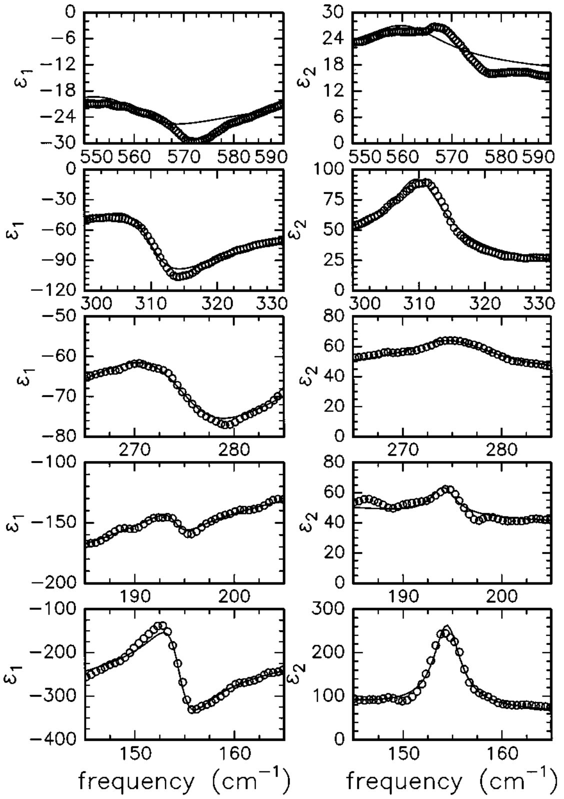

FIG. 7. Comparison of the experimental ϵ_1 and ϵ_2 for sample Ba138 (circles) and simultaneous least-squares fit of Lorentzian profiles (as described in the text) to $\epsilon_1(\omega)$ and $\epsilon_2(\omega)$ (solid lines) for the modes at 155, 190, 280, 310, and 565 cm^{-1}.

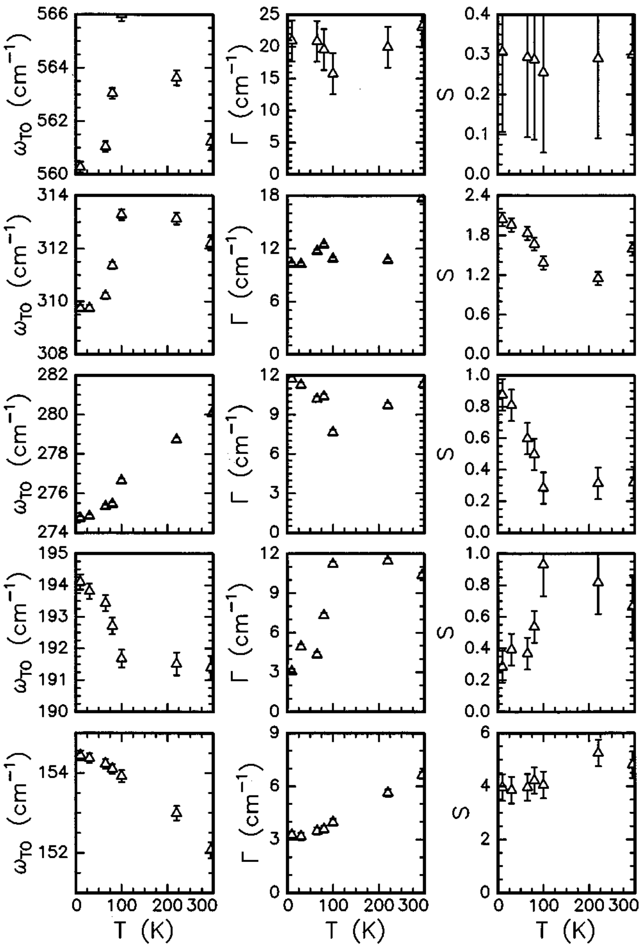

FIG. 8. Temperature dependence of the TO frequency (ω_{TO}), full width at half maximum (Γ) and the oscillator strength (S) for the observed B_{1u} modes of sample Ba138. A similar behavior is found for all samples investigated.

In total we observed nine Raman active phonons. Their positions at 10 K are summarized for all four samples in Table II.

B. Infrared ellipsometry

The real and imaginary parts of the dielectric function of the sample Ba134 measured by far-infrared ellipsometry at 300 and 10 K are shown in Fig. 6. The spectra look very similar for all ceramic samples discussed in this work and agree with the well known reponse of $\mathrm{YBa_2Cu_3O_7}$ ceramics.[28] Clearly visible are two contributions to the spectra: a broad electronic continuum with phonon-related structures on top of it. Five phonons at 150, 190, 280, 310, and 565 cm^{-1} can be identified. It is well established, that the modes appearing in the spectra of $\mathrm{YBa_2Cu_3O_7}$ ceramics correspond to the c polarized modes having B_{1u} symmetry.[4,29] Comparing the room and the low-temperature data, the phonons are more pronounced at low temperature, a result of the increased phonon lifetime. Therefore fits to the low-temperature data are more reliable. The electronic background shows a temperature dependence as well. The de-

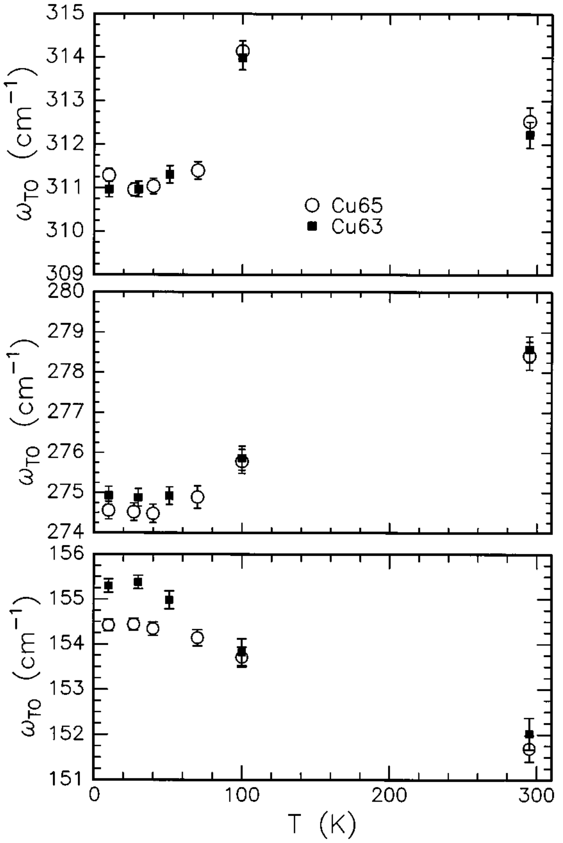

FIG. 9. Temperature dependence of the TO frequencies for the 155, 280, and 310 cm^{-1} B_{1u} modes obtained for the Cu65 (open circles) and the Cu63 sample (solid squares).

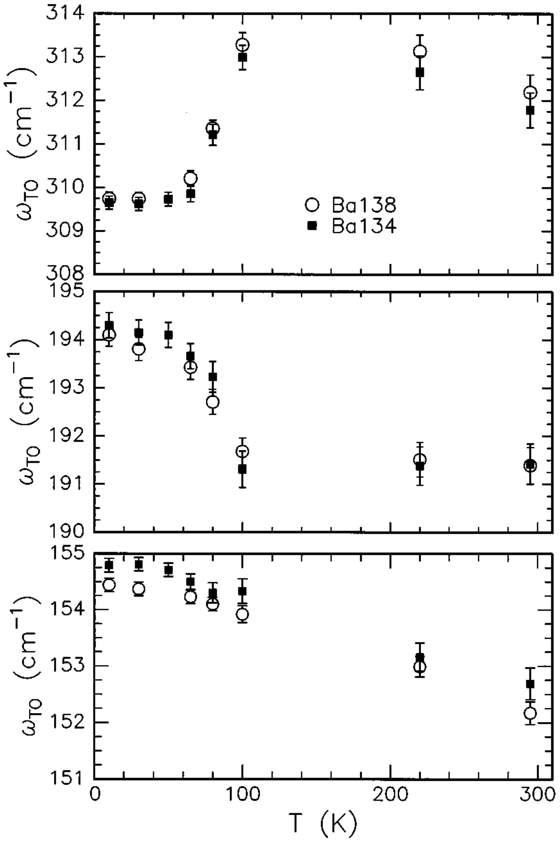

FIG. 10. Temperature dependence of the TO frequencies for the 155, 190, and 310 cm^{-1} B_{1u} modes obtained for the Ba138 (open circles) and the Ba134 sample (solid squares).

crease of $\epsilon_2(\omega)$ at low temperatures in a wide frequency regime is at least partially related to superconductivity: The contribution of superconducting carriers to the optical conductivity $[\sigma_1(\omega)=\omega\epsilon_2(\omega)/4\pi]$ is represented by a δ peak at $\omega=0$. Because of sum rules, which require the overall conservation of spectral weight, $\sigma_1(\omega)$, and thus $\epsilon_2(\omega)$, must be suppressed at finite frequencies. The steeper drop of $\epsilon_1(\omega)$ with decreasing ω in the superconducting state is directly related to the δ peak in $\sigma_1(\omega)$ by causality and therefore provides a direct experimental observation of the superconducting carriers. The electronic response is not the topic of this paper and will not be discussed further, nevertheless this observation underlines the quality of the samples investigated.

In order to determine the TO frequencies of the observed modes (ω_{TO}), we fitted Lorentzian profiles of the form

$$\tilde{\epsilon}(\omega)=\epsilon_\infty+\frac{S\omega_{TO}^2}{\omega_{TO}^2-\omega^2-i\omega\Gamma} \tag{3.1}$$

to $\epsilon_1(\omega)$ and $\epsilon_2(\omega)$ simultaneously, were S describes the oscillator strength and $1/\Gamma$ the phonon lifetime. Each mode was fitted separately, representing the background by a Drude term. The quality of the fits is demonstrated in Fig. 7, where the fitted curves are given by the solid lines. Except for the phonon at 565 cm^{-1} all modes can be well described by the Lorentzian profile. Even for $YBa_2Cu_3O_7$ crystals a non-Lorentzian line shape is well established for the 565 cm^{-1} phonon.[30,31] Because of this complicated line shape, the 565 cm^{-1} mode will not be further analyzed in this work.

The temperature dependence of the phonon parameters ω_{TO}, Γ, and S is shown for the Ba138 sample in Fig. 8; it is very similar for all other samples. The TO frequencies and their temperature dependence, including the observed anomalies, agree well with those obtained on ceramics[32] as well as on single crystals[30,31] again confirming the good quality of all our samples. The absolute values obtained for Γ and S differ from values determined on crystals, a well-known fact which can be attributed to the averaging over different oriented grains, the porosity of the samples and local field effects in the composite ceramic samples.

In the following we will focus on the TO frequencies of the modes, which are expected to show small isotopic shifts. In Fig. 9 temperature dependent TO frequencies for the 150, 280, and 310 cm^{-1} modes are displayed for samples Cu63 and Cu65. For the 150 cm^{-1} mode a systematic shift in frequency (the TO frequency for sample Cu65 is about 1 cm^{-1} lower than for sample Cu63) is detected. Also for the 280 cm^{-1} mode the TO frequencies obtained for sample Cu63 seems to be slightly higher (by about 0.5 cm^{-1}) at low temperatures than the ones obtained for sample Cu65. The 190 cm^{-1} phonon has not been included, since even at the lowest temperature this mode is too weak in these samples to obtain reliable TO frequencies.

TABLE III. Fitted TO frequencies determined by far-infrared ellipsometry at 10 K for all samples studied. Besides the values obtained by fitting Lorentzians to $\epsilon_1(\omega)$ and $\epsilon_2(\omega)$ simultaneously, the position of the maximum of $\epsilon_2(\omega)$ (brackets) and the position of the inflexion point of $\epsilon_1(\omega)$ (square brackets) are given.

Sample	Cu63	Cu65	Ba134	Ba138
ω_{TO_1} (cm^{-1})	155.30	154.42	154.79	154.41
	(155.68)	(154.36)	(154.76)	(154.33)
	[156.00]	[154.44]	[155.08]	[154.38]
ω_{TO_2} (cm^{-1})	–	194.48	194.30	194.10
		(194.58)	(194.43)	(194.44)
		[194.52]	[194.09]	[194.44]
ω_{TO_3} (cm^{-1})	274.88	274.36	273.84	274.73
	(274.51)	(274.05)	(274.67)	(274.80)
	[275.63]	[275.07]	[274.81]	[274.61]
ω_{TO_4} (cm^{-1})	310.97	311.29	309.65	309.74
	(311.13)	(311.26)	(309.74)	(310.53)
	[311.15]	[311.21]	[311.39]	[311.10]
ω_{TO_5} (cm^{-1})	564.72	565.88	560.53	560.27
	(565.29)	(566.96)	(567.39)	(566.87)
	[564.56]	[569.96]	[568.38]	[568.18]

For samples Ba134 and Ba138 the temperature dependent TO frequencies of the 150, 190, and 310 cm^{-1} modes are given in Fig. 10. Again for the 150 cm^{-1} mode the TO frequencies determined for the sample with the heavier isotope (Ba138) are shifted slightly to lower frequency (by about 0.5 cm^{-1}). For the other two modes, as well as for the 280 cm^{-1} phonon (not shown) no shift is detectable.

As discussed above, the most reliable fits were obtained

TABLE IV. Orthonormal eigenvectors ξ for all 15 Raman-active modes of $YBa_2Cu_3O_7$ obtained from a shell-model calculation (Refs. 13 and 14). The Y, Cu(1), and O(1) atoms do not contribute to these even parity modes because they are located at a center of inversion. Their eigenvector components are therefore zero for all modes and they are not listed here. Besides the calculated frequencies we have given experimentally obtained frequencies for sample Ba138 which comes closest to the natural composition of $YBa_2Cu_3O_7$. The frequencies of modes not observed in the spectra are given in brackets. The dominating contributions to the eigenvectors are underlined.

Symmetry	$\omega_{\mathrm{TO}}^{\mathrm{calc.}}$ (cm^{-1})	$\omega_{\mathrm{TO}}^{\mathrm{Ba138}}$ (cm^{-1})	ξ_{Ba}	$\xi_{\mathrm{Cu(2,3)}}$ ‘‘Plane’’	$\xi_{\mathrm{O(2)}}$	$\xi_{\mathrm{O(3)}}$	$\xi_{\mathrm{O(4)}}$ ‘‘Apex’’
$A_g \parallel c$	115.3	120.6	$\underline{-0.706}$	0.005	-0.029	-0.029	-0.005
	156.8	153.3	0.007	$\underline{0.703}$	-0.033	-0.042	0.053
	353.1	337	0.013	-0.022	$\underline{0.317}$	$\underline{-0.632}$	-0.015
	376.8	440	-0.038	0.045	$\underline{0.630}$	$\underline{0.312}$	0.046
	509.4	504	-0.003	-0.056	-0.032	-0.031	$\underline{0.703}$
$B_{2g} \parallel a$	(69.6)	–	$\underline{0.598}$	$\underline{0.278}$	0.014	0.145	0.210
	142.4	141.5	$\underline{0.332}$	$\underline{-0.556}$	0.010	-0.284	-0.015
	345.8	215.1	$\underline{0.179}$	$\underline{0.107}$	-0.045	0.035	$\underline{-0.673}$
	(427.8)	–	-0.005	-0.019	$\underline{0.703}$	0.059	-0.048
	(564.4)	–	-0.002	$\underline{0.306}$	0.061	$\underline{-0.627}$	0.013
$B_{3g} \parallel b$	(91.4)	–	$\underline{0.640}$	$\underline{0.251}$	0.130	0.011	0.098
	137.0	139.8	$\underline{-0.287}$	$\underline{0.575}$	$\underline{0.294}$	-0.014	0.009
	410.9	307.5	0.022	0.039	-0.088	$\underline{-0.699}$	-0.045
	(489.9)	–	0.085	0.059	-0.009	0.052	$\underline{-0.698}$
	(544.6)	–	0.006	$\underline{-0.318}$	$\underline{0.624}$	-0.093	-0.041

TABLE V. Normalized eigenvectors ξ for the infrared-active B_{1u} modes in $YBa_2Cu_3O_7$ determined from a shell-model calculation (Ref. 13 and 14). The frequencies of the modes not observed in the spectra, most likely because of their weak oscillator strength, are given in brackets. The dominating contributions to the eigenvectors are underlined.

$\omega_{TO}^{calc.}$ (cm^{-1})	ξ_Y	ξ_{Ba}	$\xi_{Cu(1)}$ "Chain"	$\xi_{Cu(2,3)}$ "Plane"	$\xi_{O(1)}$ "Chain"	$\xi_{O(2)}$	$\xi_{O(3)}$	$\xi_{O(4)}$ "Apex"
(94.7)	0.05	$\underline{-0.263}$	-0.165	$\underline{0.615}$	-0.149	-0.090	-0.113	-0.075
150.9	0.134	$\underline{-0.450}$	$\underline{0.567}$	-0.022	0.131	0.141	0.163	$\underline{0.269}$
196.2	$\underline{0.675}$	-0.138	$\underline{-0.449}$	-0.099	-0.053	$\underline{0.222}$	$\underline{0.241}$	-0.183
(307.5)	-0.119	0.001	-0.073	0.039	0.096	$\underline{-0.446}$	$\underline{0.534}$	-0.002
317.4	-0.196	-0.057	$\underline{-0.285}$	0.068	$\underline{0.912}$	0.126	-0.023	-0.014
370.2	$\underline{0.574}$	-0.019	0.180	-0.093	$\underline{0.291}$	$\underline{-0.422}$	$\underline{-0.296}$	-0.041
531.1	0.092	0.007	$\underline{-0.485}$	-0.028	-0.091	-0.074	-0.072	$\underline{0.602}$

for the data taken at the lowest temperature. In order to confirm the small shifts, we extracted TO frequencies from the 10 K data applying two additional methods: we determined the maximum of $\epsilon_2(\omega)$ by fitting a fourth-order polynomial to the maximum of the absorbtion peak and we determined the inflexion point of $\epsilon_1(\omega)$ by fitting a fourth-order polynomial to the region arround the inflexion point. Within the approximation of Lorentzian oscillators with a small damping, the maximum of $\epsilon_2(\omega)$, the inflexion point of $\epsilon_1(\omega)$ and the TO frequency should coincide. In Table III the 10 K values of the TO frequency determined from a Lorentz fit to $\epsilon_1(\omega)$ and $\epsilon_2(\omega)$ simultaneously, the maximum frequency of $\epsilon_2(\omega)$ (brackets) and the inflexion point of $\epsilon_1(\omega)$ (square brackets) are given for all modes and all samples . Except for the 565 cm^{-1} mode the frequencies determined with different methods agree well, indicating that Lorentzian profiles provide a good description of the measurements.

IV. ANALYSIS AND DISCUSSION

A. Frequency shifts and eigenvectors

In an earlier publication the effect of the $^{63}Cu \leftrightarrow {}^{65}Cu$ substitution on the A_g modes at 121 and 154 cm^{-1} has been analyzed with a model of two coupled modes involving Ba and Cu(2,3), respectively.[12] This analysis, which will not be repeated here, revealed the 154 cm^{-1} mode to be an almost pure Cu vibration (Ba admixture $<20\%$), while the Cu admixture to the 121 cm^{-1} mode was shown to be very small. This confirmed the qualitative results of earlier Raman measurements on the Cu isotope effect by Mascarenhas *et al.*[10] and Irwin *et al.*[11] and is also consistent with the resonant Raman scattering results of Heyen *et al.*.[27] With our new data we are able to give slightly improved values for the Ba-Cu-A_g mode coupling: Using the coupled two-mode model and the experimental frequencies at 10 K of the two A_g phonons of all four measured samples a least-squares fit

TABLE VI. Experimental shifts of Raman phonon frequencies obtained by isotopic replacement of Cu and Ba, compared to predictions based on lattice dynamical calculations.

		Experiment		Theory	
Symmetry	ω^{calc} (cm^{-1})	$\Delta\omega(^{63}Cu/^{65}Cu)$ (cm^{-1})	$\Delta\omega(^{134}Ba/^{138}Ba)$ (cm^{-1})	$\Delta\omega(^{63}Cu/^{65}Cu)$ (cm^{-1})	$\Delta\omega(^{134}Ba/^{138}Ba)$ (cm^{-1})
A_g	115	$0.2\pm.2$	$1.3\pm.2$	0	1.5
A_g	157	$2.1\pm.2$	$0.1\pm.2$	2.4	0
A_g	353	0 ± 1	0 ± 1	0	0
A_g	377	0 ± 1	0 ± 1	0	0
A_g	501	0 ± 1	0 ± 1	0	0
B_{2g}	142	$0.7\pm.5$	$0.4\pm.5$	1.0	0.3
B_{3g}	137	$1.3\pm.5$	$0\pm.5$	1.0	0.2
B_{2g}	346	0 ± 1	0 ± 1	0	0
B_{3g}	490	0 ± 1	0 ± 1	0	0

TABLE VII. Experimental shifts of the infrared active B_{1u} phonons of $YBa_2Cu_3O_7$ obtained by isotopic replacement of Cu and Ba in comparison with predictions from lattice dynamical calculations. The error bars of the experimental shifts are estimated to be ±0.25.

	Experiment		Theory	
Mode	$\Delta\omega_{TO}(^{63}Cu/^{65}Cu)$ (cm^{-1})	$\Delta\omega_{TO}(^{134}Ba/^{138}Ba)$ (cm^{-1})	$\Delta\omega_{TO}(^{63}Cu/^{65}Cu)$ (cm^{-1})	$\Delta\omega_{TO}(^{134}Ba/^{138}Ba)$ (cm^{-1})
150 cm^{-1}	1	0.6	0.77	0.71
190 cm^{-1}	–	0	0.68	0.08
280 cm^{-1}	0.5	0	0.45	0
310 cm^{-1}	0	0	0.28	0.02
565 cm^{-1}	–	–	1.98	0

of the eigenvectors yields a Cu admixture lower than 15% for the 121 cm^{-1} phonon and a Ba admixture smaller than 15% for the 153 cm^{-1} phonon. This mixing does not appear to change with temperature and thus remains weak in the entire range from 10 K to room temperature.

If more than two unequivalent atoms are involved in a vibrational mode, the situation becomes more complex. Applying first-order perturbation theory, the frequency shift due to the change of the mass of the ith atom is shown to be proportional to the square modulus of the ith component of the corresponding eigenvector:[33,34]

$$\frac{\partial\omega_n}{\partial m_i} = -\frac{\omega_n}{2m_i}[|\xi_{i,x}|^2+|\xi_{i,y}|^2+|\xi_{i,z}|^2]. \tag{4.1}$$

Here ω_n represents the frequency of mode n, m_i corresponds to the mass of atom i, and $\xi_{i,j}(n)$ gives the ith component of the orthonormal eigenvector of mode n along the direction j. From Eq. (4.1) it becomes immediately clear that the observation of phonon frequency shifts when changing the mass of certain atoms i probes the mode eigenvectors.

In the following we take phonon eigenvectors obtained from a shell-model calculation.[13,14] We compare the observed frequency shifts with those predicted by Eq. (4.1). Details of the lattice dynamical calculation as well as a comparison of the calculated frequencies with those observed for the Raman- and infrared-active modes of $YBa_2Cu_3O_7$ are given in Ref. 13. The orthonormal eigenvectors are given in Table IV for the Raman-active modes and in Table V for the infrared-active B_{1u} modes having c polarization. We use the following (standard) nomenclature for the different sites in the $YBa_2Cu_3O_7$ unit cell: The Cu atoms located in the chains are denoted by Cu(1), whereas the Cu atoms in the planes are given by Cu(2) and Cu(3). O(1) denotes the chain oxygen atoms, O(2) and O(3) are those in the planes, located on the a and b axis, respectively. The apical oxygens are represented by O(4). A schematic view of these eigenvectors is given in Ref. 13.

A first test for the calculated eigenvectors of the Raman-active modes are the 121 cm^{-1} and 154 cm^{-1} modes discussed above. The Ba and Cu eigenvector components, respectively, are close to $1/\sqrt{2}$, which is the value one would expect for a pure vibration of one sublattice having two atoms in its primitive cell. The calculations of Ref. 13 thus predict only a very weak coupling between these vibrations. In Table VI the experimentally observed shifts of the Raman mode frequencies are given together with the ones calculated

TABLE VIII. Experimental shifts of B_{1u} phonon frequencies in $YBa_2Cu_3O_7$ obtained by rare earth and oxygen replacement taken from Ref. 7, compared to predictions of lattice dynamical calculations.

	Experiment		Theory	
Mode	$\Delta\omega_{TO}$ (Y/Er) (cm^{-1})	$\Delta\omega_{TO}(^{16}O/^{18}O)$ (cm^{-1})	$\Delta\omega_{TO}$ (Y/Er) (cm^{-1})	$\Delta\omega_{TO}(^{16}O/^{18}O)$ (cm^{-1})
150 cm^{-1}	4.1	2.9	0.75	2.38
190 cm^{-1}	31.2	1	23.78	3.46
280 cm^{-1}	5.2	13.5	3.35	16.72
310 cm^{-1}	7.3	12.6	32.27	14.07
565 cm^{-1}	0.9	20.4	1.24	24.48

TABLE IX. Comparison of experimental TO frequencies ($\omega_{\mathrm{TO}}^{\mathrm{expt}}$) and oscillator strengths (S^{expt}) of the B_{1u} vibrational modes of $\mathrm{YBa_2Cu_3O_7}$ crystals (Ref. 38) with values obtained from lattice dynamical calculations. The oscillator strength S^{calc} was determined from Eq. (4.2) making use of the charges assumed for the calculation.

$\omega_{\mathrm{TO}}^{\mathrm{expt}}$ (cm^{-1})	S^{expt}	$\omega_{\mathrm{TO}}^{\mathrm{calc.}}$ (cm^{-1})	$S^{\mathrm{calc.}}$
155.0	10.2	150.9	3.78
195.6	1.0	196.2	0.40
286.2	1.4	317.4	1.04
314.9	2.8	370.2	1.07
565.0	0.5	531.1	0.23

from the eigenvectors. The agreement between calculation and experiment for the two low frequency A_g modes is very good. The experiments also reveal a significant Cu contribution to the B_{2g} mode at 142 cm^{-1} and to the B_{3g} mode at 140 cm^{-1}. The behavior of the B_{2g} mode is well described by the calculated eigenvectors which yield a Cu contribution of about 60%. The effect of Cu substitution on the B_{3g} mode is even better described by the eigenvectors and yields a Cu contribution of 66%. All other observed modes have frequencies above 300 cm^{-1} and show neither a shift with $^{63}\mathrm{Cu}\leftrightarrow{}^{65}\mathrm{Cu}$ nor with $^{134}\mathrm{Ba}\leftrightarrow{}^{138}\mathrm{Ba}$ substitution: because of the larger mass of the cations only the much lighter oxygen atoms contribute to these high frequency modes. The experimental observations are consistent with the calculated eigenvectors which contain only small contributions of Ba and Cu to the higher frequency Raman modes.

Concerning the infrared-active modes, the data which allow the determination of the TO frequencies with the highest accuracy are the ones taken at the lowest temperature (10 K). The shifts of the TO frequencies of the B_{1u} modes at 10 K are given in Table VII together with the shifts calculated using the eigenvectors of Table V. Only the 150 cm^{-1} mode is found to be affected by the Ba substitution; the absolute shift estimated from the eigenvector agrees well with the measured one, indicating that the calculated Ba contribution of 40% to this mode is correct. An influence of Cu substitution is seen on the TO frequencies of the 150 and 280 cm^{-1} modes which is again in good agreement with the calculation. The Cu contributions to these modes extracted from the eigenvectors are 32% for the 150 cm^{-1} mode and 9% for the 280 cm^{-1} mode. The fact, that no shift is observed for the 310 cm^{-1} mode is, within the experimental error, compatible with the calculated eigenvectors. For the 190 cm^{-1} and 565 cm^{-1} modes it was not possible to extract reliable frequencies from the data. Shifts of these modes for $^{63}\mathrm{Cu}\leftrightarrow{}^{65}\mathrm{Cu}$ substitution are, however, predicted from the eigenvectors.

TABLE X. Effective charges $e_{t_X}^{*}$ of atoms X calculated from measured oscillator strengths using the eigenvectors of Table V (in units of e). In order to estimate the uncertainties of the effective charges given, we varied the oscillator strengths by ±10%. Most sensitive turned out to be the values for Y and Ba. From this we conluded the errors of the numbers to be given by $\Delta e_{t_{\mathrm{Y}}}^{*}\approx\pm0.8$; $\Delta e_{t_{\mathrm{Ba}}}^{*}\approx\pm0.5$; $\Delta e_{t_{\mathrm{Cu}}}^{*}\approx\pm0.4$, and $\Delta e_{t_{\mathrm{O(1)}}}^{*}\approx\Delta e_{t_{\mathrm{O(2,3)}}}^{*}\approx\Delta e_{t_{\mathrm{O(4)}}}^{*}\approx\pm0.25$.

Effective charges					
$e_{t_{\mathrm{Y}}}^{*}$	$e_{t_{\mathrm{Ba}}}^{*}$	$e_{t_{\mathrm{Cu}}}^{*}$	$e_{t_{\mathrm{O(1)}}}^{*}$	$e_{t_{\mathrm{O(2,3)}}}^{*}$	$e_{t_{\mathrm{O(4)}}}^{*}$
2.84	3.94	2.23	−1.71	−2.51	−2.84

Some experimental data have been reported concerning the effects of oxygen isotopic exchange ($^{16}\mathrm{O}\leftrightarrow{}^{18}\mathrm{O}$) on infrared active modes and the effects of replacing yttrium by other rare-earth elements.[4,6,7] The assignment of the B_{1u} modes is mainly based on these experiments: the rare earth atoms were shown to contribute considerably to the 190 cm^{-1} vibration, whereas the 280, 310, and 565 cm^{-1} modes were shown to be mostly oxygen related. In particular the phonon at 280 cm^{-1} was concluded to be mostly due to a vibration of chain oxygen atoms. In the following we will show, that the quantitative results of these experiments are compatible with the set of eigenvectors presented here. For the rare earth substitution we focus on the replacement of Y by Er. Since the change of lattice parameters is very small[35] ($\mathrm{YBa_2Cu_3O_7}$: $a=3.8198$ Å; $b=3.8849$ Å; $c=11.6762$ Å, and $\mathrm{ErBa_2Cu_3O_7}$: $a=3.8127$ Å; $b=3.8785$ Å; $c=11.6656$ Å), the effect on the phonon modes should be most likely related to the change of mass. Neglecting chemical effects on bond lengths and force constants, one can perform a similar analysis as for the isotope experiments. However, because of the large change of the mass ($m_{\mathrm{Y}}=88.91$; $m_{\mathrm{Er}}=167.26$) it is questionable whether the problem can still be handled within first-order perturbation theory.

In Table VIII experimentally observed shifts of the B_{1u} modes for the Y↔Er and the $^{16}\mathrm{O}\leftrightarrow{}^{18}\mathrm{O}$ exchange, determined by Crawford *et al.*,[7] are displayed together with values calculated from the eigenvectors of Table V. For the $^{16}\mathrm{O}\leftrightarrow{}^{18}\mathrm{O}$ substitution a good agreement between theory and experiment is found. However, most measured shifts are slightly smaller than the theoretical ones. This may indicate that oxygen was not fully replaced in these samples. Qualitatively the agreement between theory and experiment for the rare earth substitution is good, however, the quantitative discrepancies are larger than for the substitution experiments discussed above. In particular, the shift for the 310 cm^{-1} mode is strongly overestimated by the calculation, while that of the 150 cm^{-1} phonon is much too small. As mentioned earlier, this might have its origin in the failure of the perturbative approach used because of the large change of mass.

B. Effective charges

The oscillator strengths of infrared active phonon modes are related to the dipole moment arising from the displacement of the ions involved in a vibration. In particular, the oscillator strength (S_j) is proportional to the ratio of the electric polarization energy to the mechanical energy of the mode j:[36]

$$S_j=\frac{4\pi}{V}\frac{[\Sigma_i e^*_{t_i} u_{ij}]^2}{\omega^2_{\mathrm{TO}_j}\Sigma_i m_i u^2_{ij}}. \tag{4.2}$$

In this relation $e^*_{t_i}$ and m_i correspond to the effective charge and mass of atom i, respectively, u_{ij} represents the displacement of particle i in mode j with the TO frequency ω_{TO_j}, while the unit cell volume occupied by the atoms i is given by V (the displacements u are related to the eigenvectors ξ by $u=\xi/\sqrt{m_i}$, where m_i is the mass of the atom under consideration.). By inversion of this relation effective charges of the atoms can be extracted as has been recently demonstrated for the La_2CuO_4 system.[37] In the following we determine effective charges by making use of the eigenvectors which have just been shown to describe rather well the isotope shifts of the phonon frequencies in $YBa_2Cu_3O_7$. As experimental input we use the phonon parameters (ω_{TO} and S) of the five observed B_{1u} modes of a (natural) $YBa_2Cu_3O_7$ crystal, which we have published earlier.[38] These parameters, obtained at 300 K, are given in Table IX. The primitive cell ($V=173.27$ Å^3) contains one formula unit. The analysis presented accounts for six different effective charges: $e^*_{t_{\mathrm{Y}}}$ for the Y atom, $e^*_{t_{\mathrm{Ba}}}$ for the Ba atoms, $e^*_{t_{\mathrm{Cu}}}$ for all Cu atoms, $e^*_{t_{\mathrm{O(1)}}}$ for the chain oxygen atom, $e^*_{t_{\mathrm{O(2,3)}}}$ for the in-plane oxygen atoms, and $e^*_{t_{\mathrm{O(4)}}}$ for the apical oxygens. Equation (4.2) applied to all five observed B_{1u} modes, together with the electric charge neutrality condition, $\Sigma_i e^*_{t_i}=0$, yields a set of six linear equations for the six unknown effective charges.

The effective charges obtained from this procedure are given in Table X. The value obtained for Ba is much larger than its nominal valence charge (+2, sometimes called static charge). Those of O(2,3) and O(4), which are related to Ba by charge neutrality, have also charges with absolute values larger than 2. However, dynamic contributions to these charges are expected to occur. In view of this fact and of the experimental uncertainties, the values obtained seem reasonable. Significantly lower values of $e^*_{t_{\mathrm{O(1)}}}$ compared to $e^*_{t_{\mathrm{O(4)}}}$ were also observed by Masterov *et al.*[39] from NMR and Mössbauer spectroscopy and by Cava *et al.*,[40] where elastic neutron scattering revealed interatomic distances which are measures of the amount of charge in the chemical bond between the atoms. This observation was interpreted as an indication that holes are placed mainly at the chain oxygen sites. A calculation of dynamical effective charges based on the electronic band structure[41] would be highly desirable.

V. CONCLUSION

We have investigated the effect of ^{134}Ba↔^{138}Ba and ^{63}Cu↔^{65}Cu isotopic substitution on the optical phonons in $YBa_2Cu_3O_7$ ceramics using Raman spectroscopy and far-infrared ellipsometry. The observed shifts of the phonon frequencies agree well with predictions based on eigenvectors obtained from lattice dynamical calculations and reveal their relative Ba and Cu content: the 121 cm^{-1} (150 cm^{-1}) A_g mode was confirmed to be an almost pure Ba (Cu) vibration with a contribution of Cu (Ba) to the eigenvectors of less than 15%. For the 142 cm^{-1} B_{2g} mode and for the 140 cm^{-1} B_{3g} mode a Cu contribution of the order of 60% was found, whereas for the 353, 376, and 509 cm^{-1} A_g modes and for the 210 cm^{-1} B_{2g} and 308 cm^{-1} B_{3g} phonons neither a Cu nor a Ba contribution to the vibration was detectable. For the infrared-active 150 cm^{-1} B_{1u} mode a Ba contribution on the order of 40% is observed, while for this mode a Cu admixture of 30% and for the 280 cm^{-1} mode a Cu admixture of about 10% was found. Neither a shift of the 190, 280, 310 cm^{-1} modes for Ba substitution nor a shift of the 310 cm^{-1} mode was detectable with Cu substitution, indicating that the Ba and Cu admixtures, respectively, are negligible for these modes. Earlier experiments concerning the ^{16}O↔^{18}O substitution and Y↔Er exchange are compatible with the same set of eigenvectors. Using this set of eigenvectors we extracted dynamic effective charges for all atoms in the unit cell from previously measured infrared oscillator strengths. We find that the absolute value of the charge of the chain oxygens is smaller than that of the apical oxygens. This is compatible with results extracted from NMR and Mössbauer spectroscopy data as well as with results obtained from the interatomic distances determined by elastic neutron scattering. If the transverse charges are attributed to a static charge, we can conclude that holes are also located at the chain oxygen sites.

ACKNOWLEDGMENTS

We are grateful to W. Kress for providing us with the numerical results of the calculations presented in Ref. 13. We thank D. Böhme, H. Hirt, and M. Siemers for technical assistance. We would like to acknowledge the assistance of E. Winckler in the sample preparation. Thanks are also due to J. Humlíček and T. Ruf for a careful reading of the manuscript, and E. Sherman for pointing out additional theoretical work related to the topic (Refs. 42 and 43).

---

[1] C. Thomsen and M. Cardona, in *Physical Properties of High Temperature Superconductors I*, edited by D.M. Ginsberg (World Scientific, Singapore, 1989), p. 464, and references therein.

[2] D. Strauch and B. Dorner, J. Phys. C **19**, 2853 (1986).

[3] C. Thomsen, in *Light Scattering in Solids VI*, edited by M. Cardona and G. Güntherodt (Springer, Berlin, 1991), p. 326.

[4] A.P. Litvinchuk, C. Thomsen, and M. Cardona, in *Physical Properties of High Temperature Superconductors IV*, edited by D.M. Ginsberg (World Scientific, Singapore, 1994), p. 375.

[5] M. Cardona, *Festkörperprobleme 34, Advances in Solid State Physics* (Vieweg, Braunschweig, 1994), p. 35.

[6] M. Cardona, R. Liu, C. Thomsen, W. Kress, E. Schönherr, M. Bauer, L. Genzel, and W. König, Solid State Commun. **67**, 789 (1988).

[7] M.K. Crawford, W.E. Farneth, E.M. McCarron III, and R.K.

Bordia, Phys. Rev. B **38**, 11 382 (1988).

[8] C. Thomsen, A.P. Litvinchuk, E. Schönherr, and M. Cardona, Phys. Rev. B **45**, 8154 (1992).

[9] D. Zech, H. Keller, K. Conder, E. Kaldis, E. Liarokapis, N. Poulakis, and K.A. Müller, Nature **371**, 681 (1994).

[10] A. Mascarenhas, H. Katayama-Yoshida, J. Pankove, and S.K. Deb, Phys. Rev. B **39**, 4699 (1989).

[11] J.C. Irwin, J. Chrzanowski, E. Altendorf, J.P. Franck, and J. Jung, J. Mater. Res. **5**, 2780 (1990).

[12] T. Strach, T. Ruf, E. Schönherr, and M. Cardona, Phys. Rev. B **51**, 16 460 (1995).

[13] J. Humlíček, A.P. Litvinchuk, W. Kress, B. Lederle, C. Thomsen, M. Cardona, H.-U. Habermeier, I.E. Trofimov, and W. König, Physica C **206**, 345 (1993).

[14] W. Kress (private communication).

[15] Obtained from Trace Sciences, Inc., Scarborough, Ont. Canada M1W 3W6.

[16] E. Schönherr, Mater. Res. Bull. **23**, 1211 (1988).

[17] E. Schönherr, Solid State Ion. **32/33**, 1080 (1989).

[18] C. Thomsen, R. Liu, M. Bauer, A. Wittlin, L. Genzel, M. Cardona, E. Schönherr, W. Bauhofer, and W. König, Solid State Commun. **65**, 55 (1988).

[19] K.L. Barth, D. Böhme, K. Kamaras, F. Keilmann, and M. Cardona, Thin Solid Films **234**, 314 (1993).

[20] A. Röseler, *Infrared Spectroscopic Ellipsometry* (Akademie Verlag, Berlin, 1990).

[21] D. Miller and P.L. Richards, Phys. Rev. B **47**, 12 308 (1993).

[22] R.M.A. Azzam and N.M. Bashara, *Ellipsometry and Polarized Light* (North-Holland, Amsterdam, 1977).

[23] H. Rosen, E.M. Engler, T.C. Strand, V.Y. Lee, and D. Bethune, Phys. Rev. B **36**, 726 (1987).

[24] U. Fano, Phys. Rev. **124**, 1866 (1961).

[25] K.F. McCarty, J.Z. Liu, R.N. Shelton, and H.B. Radousky, Phys. Rev. B **41**, 8792 (1990).

[26] B. Friedl, C. Thomsen, H.-U. Habermeier, and M. Cardona, Solid State Commun. **81**, 989 (1992).

[27] E.T. Heyen, S.N. Rashkeev, I.I. Mazin, O.K. Andersen, R. Liu, M. Cardona, and O. Jepsen, Phys. Rev. Lett. **65**, 3048 (1990).

[28] T. Timusk and D.B. Tanner, in *Physical Properties of High Temperature Superconductors I*, edited by D.M. Ginsberg (World Scientific, Singapore, 1989), p. 339.

[29] M. Bauer, Ph.D. thesis, Universität Tübingen, 1990.

[30] J. Schützmann, S. Tajima, S. Miyamoto, Y. Sato, and R. Hauff, Phys. Rev. B **52**, 13 665 (1995).

[31] C.C. Homes, T. Timusk, D.A. Bonn, R. Liang, and W.N. Hardy, Can. J. Phys. (to be published).

[32] L. Genzel, A. Wittlin, M. Bauer, M. Cardona, E. Schönherr, and A. Simon, Phys. Rev. B **40**, 2170 (1989).

[33] A. Debernardi and M. Cardona, Phys. Rev. B **54**, 11 305 (1996).

[34] J. Menéndez, J.B. Page, and S. Guha, Philos. Mag. B **70**, 651 (1994).

[35] R.M. Hazen, in *Physical Properties of High Temperature Superconductors II*, edited by D.M. Ginsberg (World Scientific, Singapore, 1990).

[36] J.W. Powell, G.S. Edwards, L. Genzel, F. Kremer, A. Wittlin, W. Kubasek, and W. Peticolas, Phys. Rev. A **35**, 3929 (1987).

[37] R. Henn, J. Kircher, and M. Cardona, Physica C **269**, 99 (1996).

[38] J. Kircher, R. Henn, M. Cardona, P.L. Richards, and G.P. Williams, J. Opt. Soc. Am. B (to be published).

[39] V.F. Masterov, P.P. Seregin, F.S. Nasredinov, N.P. Seregin, and M.A. Sagatov, Phys. Status Solidi B **196**, 11 (1996).

[40] R.J. Cava, A.W. Hewat, B. Batlogg, M. Marezio, K.M. Rabe, J.J. Krajewski, W.F. Peck Jr., and L.W. Rupp Jr., Physica C **165**, 419 (1990).

[41] J. Bennetto and D. Vanderbilt, Phys. Rev. B **53**, 15 417 (1996).

[42] E. Sherman, Physica C **216**, 439 (1993).

[43] E. Sherman, Z. Phys. B **98**, 489 (1995).